

In situ formation of electrospun graphene nanofibers

Jules Brehme, Markus Gruschwitz, Christoph Tegenkamp, Franz Renz, Ralf Franz Sindelar

Suggested citation:

Brehme, Jules, Markus Gruschwitz, Christoph Tegenkamp, Franz Renz, and Ralf Franz Sindelar. 2025. "In situ formation of electrospun graphene nanofibers." *Journal of Materials Science* 60 (27): 11446–56. <https://doi.org/10.25968/opus-3641>.

Abstract


Graphene-based materials are currently in the focus of research, but toward any application a simple and reliable fabrication process is mandatory. To date, graphene nanofibers (GNF) made via electrospinning have been established, using graphene oxide (GO) as templating agent. However, relying on GO as a solid insoluble precursor makes the process harder. We present a method to produce in situ neat GNFs made of solely electrospun polyacrylonitrile (PAN). Besides heating in an oven up to 1700 °C, the GNFs were heated by self-resistive heating. For this the nanofibers were placed into an electrical circuit and a rising electrical power was applied reaching over 3200 °C directly in the nanofibers. The Raman, XPS, and XRD results show high crystalline GNFs, with little to no defects and high graphitization degree. Furthermore, the electrical transport measurements revealed an eightfold increase in the conductivity. The deeper analysis of the 2D-band indicates the graphene structure. This simple way of electrospun GNFs with a commonly used polymer precursor opens the door to easier access and broader functional application of said nanofibers.

Terms of use

CC BY 4.0



In situ formation of electrospun graphene nanofibers

Jules Brehme^{1,2,3,*} , Markus Gruschwitz⁴, Christoph Tegenkamp⁴, Franz Renz^{1,3}, and Ralf Franz Sindelar^{2,3}

¹Institute of Inorganic Chemistry, Leibniz University Hannover, Callinstrasse 9, 30167 Hannover, Germany

²Electrospinning Laboratory, Hochschule Hannover, Ricklinger Stadtweg 120, 30519 Hannover, Germany

³Hannover School for Nanotechnology, Laboratory for Nano- and Quantumengineering, Schneiderberg 39, 30167 Hannover, Germany

⁴Institute for Physics, TU Chemnitz, Reichenhainer Strasse 70, 09126 Chemnitz, Germany

Received: 6 February 2025

Accepted: 2 June 2025

Published online:
16 June 2025

© The Author(s), 2025

ABSTRACT

Graphene-based materials are currently in the focus of research, but toward any application a simple and reliable fabrication process is mandatory. To date, graphene nanofibers (GNF) made via electrospinning have been established, using graphene oxide (GO) as templating agent. However, relying on GO as a solid insoluble precursor makes the process harder. We present a method to produce in situ neat GNFs made of solely electrospun polyacrylonitrile (PAN). Besides heating in an oven up to 1700 °C, the GNFs were heated by self-resistive heating. For this the nanofibers were placed into an electrical circuit and a rising electrical power was applied reaching over 3200 °C directly in the nanofibers. The Raman, XPS, and XRD results show high crystalline GNFs, with little to no defects and high graphitization degree. Furthermore, the electrical transport measurements revealed an eightfold increase in the conductivity. The deeper analysis of the 2D-band indicates the graphene structure. This simple way of electrospun GNFs with a commonly used polymer precursor opens the door to easier access and broader functional application of said nanofibers.

Introduction

Carbon is one of the most abundant elements on Earth and has a wide variety of allotrope forms it presents, due to its four valence electrons and the hybridization states it can have. Therefore, versatile carbon (nano-) materials have been the subject of research for a long time. Various carbon nanomaterials have been synthesized and brought into a broad range of applications

due to their versatility in properties. Among them the dependencies the dimension, e.g., fullerenes such as C₆₀ (0 dimensional), carbon nanotubes (CNT) and nanofibers (CNF) (1D), or graphene nanosheets (2D) and diamonds (3D), also influences the usability, as each of those provide a unique shape, structure, and therefore characteristic properties [1]. These allotropes and their combinations are used to synthesize new hybrid materials with unique properties [2, 3]. Fibers

Handling Editor: Kevin Jones.

Address correspondence to E-mail: jules.brehme@hs-hannover.de

E-mail Addresses: markus.gruschwitz@physik.tu-chemnitz.de; christoph.tegenkamp@physik.tu-chemnitz.de; franz.renz@acd.uni-hannover.de; ralf.sindelar@hs-hannover.de

made of graphene are uncommon up to today. Additionally, those graphene fibers (GF) are prepared out of processing macroscopic graphene oxide (GO) in an aqueous solution, where the formation of GF took place upon the reduction of the GO fibers [4]. Another combination of these is the fabrication of graphene nanofibers (GNFs) out of electrospun GO in a polyarylenesulfone (PAS) solution, which was then heated to 3000 °C in an argon flow to get neat GNFs [5]. It is important to note that those publications use a templating approach, with a high weight percentage of GO's, for the GNF production and that due to the sheet structure of the GO the fiber structure is impaired with all the folds and wrinkles instead of a smooth surface. This forms a great incentive to use other alternatives for precursors to use, as GO requires extra precursor production, which is costly and present an additional environmental issue, using the chemicals to produce said GO. Additionally, the use of a single material simplifies the production process, especially for scale-up.

Electrospinning is an uncomplicated, well known, and cost-effective method to fabricate fibers, with a potential to scale-up, compared to vapor growth, spraying, or catalyst supported growth. Although the typical fibers in this process exceed the 100 nm range, they are still called nanofibers in the aspect of engineering and in the industry [6]. In a typical electrospinning process, a potential difference is applied between a droplet of a polymer solution contained in a syringe and a grounded collector. In our case, we use a rotating collector to get highly aligned fibers as it has been previously reported that the bulk conductivity, the conductivity of CNF paper, and graphitization degree, the ratio of the D- and G-band in the Raman spectra, of the nanofibers are dependent on the alignment [7]. Once the Coulomb forces acting on the droplet overcome its surface tension, a fiber jet emerges from the apex of the conical meniscus known as the Taylor cone [8]. The fiber solvent vaporizes, and the jet solidifies during the flight to the collector and the solid nanofibers are then stabilized at 250 °C in an air atmosphere, which is also known as the cyclization step for PAN and furthermore carbonized to obtain CNFs [7]. With the high surface-to-volume ratio, good thermal, and electrical conductivity, mechanical properties of the CNF are highly expected materials in the near future [2]. With their high surface-to-volume ratio and the controllable structure, electrospun nanofibers produced by electrospinning have been reportedly used in

biomedical engineering, with higher surface performance in post-operative adhesion [9, 10] and can be explored in smart textile production [11] or in digital information transport [12, 13].

On the other side is graphene, re-discovered in 2004 [14], as a monolayer of sp^2 -bonded carbon atoms ordered in a two-dimensional honeycomb lattice, which has unique physical properties. It has a tensile strength over 100 times greater than steel and is the material with the highest thermal conductivity known so far. Furthermore, it is an excellent electrical conductor and is impermeable to gases and liquids [15, 16]. Due to these properties, graphene is an important candidate for various applications such as sensors, transparent electrodes for diodes or photovoltaics, or composites [17]. Its characteristics can be analyzed using Raman spectroscopy; i.e., in the case of a single-layer graphene, two sharp peaks, the G-band and the 2D-band, are observed. The 2D-band is, in that case, sharp as well as symmetrical, centered around 2700 cm^{-1} [18]. With an increasing number of layers, the 2D-band broadens and becomes asymmetric, while the full width at half-maximum (FWHM) is a quantitative guide to determine the layer numbering of few-layer graphene (FLG)[19, 20].

Typical synthesis of graphene is done either by mechanical cleavage from highly oriented pyrolytic graphite (HOPG) [14], reduction of GO, chemical vapor deposition, or atomic carbon extraction from HOPG through a metal layer[21], as well as thermal treatment of polymers [22]. In this paper, we achieved to synthesize in situ GNFs out of CNFs instead of using GO as a template and validate our claim using Raman spectroscopy, X-ray diffraction, and XPS, comparing these to typical CNFs. Additionally, 4-point probe transport measurements were performed to determine the electrical conductivity of our GNFs. We show a simple method to create GNFs out of CNF with just the usage of electrospun PAN as precursor material. For this, we take advantage of the self-heating of the CNFs during the application of electrical power using gallium as a contacting agent. This step is only possible after carbonization, as the previous material iterations are not electrically conductive. PAN was chosen for its simple use during the electrospinning process, due to the broad spinning window, with the concentration ranging from 4 wt% to 14 wt%, and a voltage window of 6 kV to 30 kV. These GNFs may be used for advanced composites, electrodes, or catalysts.

Materials and methods

Materials

Polyacrylonitrile (PAN), as powder form from Sigma-Aldrich with a molecular weight of 150,000 Mw, was used as precursor for the carbon nanofiber (CNF) fabrication. N,N Dimethylformamide (DMF) was used as solvent supplied by Carl Roth. For both carbonization and graphenization, a mixture of 2 % H₂/98 % Ar was used, supplied by Westfalen AG. For the power supply, a Voltcraft DPPS-60-15 with a maximum output of 900 W was used.

Preparation of nanofibers

The complete process for the fabrication of GNFs comprises four stages. At first, PAN was dissolved in DMF by 16 wt% and stirred for 12 h to obtain a homogeneous solution. This solution was then electrospun at 18 kV with a rate of 1 mL h⁻¹, a needle to collector distance of 20 cm and a collector speed of 10 ms⁻¹.

For the second stage, the spun fibers were stabilized at 250 °C with a heating and cooling rate of 1 °Cmin⁻¹, and the 250 °C were hold for 5 h. For the successful cyclization, the fibers were mechanically strained during the process.[7]

The third stage is the carbonization step in which the nanofibers were pyrolyzed at 1700 °C for an hour with a ramp rate of 5 °Cmin⁻¹ while being in a reduced atmosphere of 2 % H₂/98 % Ar. As reference typical CNF with carbonization temperatures at 800 °C and 1700 °C, respectively, were prepared as well.

Lastly, the obtained CNF were placed into an electric circuit using gallium as contacting agent between the CNF and the Cu wires. To ensure that no oxygen

was present, a low-pressure (200 mbar) H₂/Ar(2%/98%) -atmosphere was established. To ensure the processing of the CNF is successful, the fibers should contain as little defects as possible after the carbonization. Especially bend and partially broken samples were not suitable to be processed. After that, the voltage of the power supply was increased in several increments to get a power of 27 W. This has been hold for 15 min before increasing to 97,3 W for 2 h. The temperature uniformity during graphenization was established during this step, controlled by the observation of the color of the fibers. Lastly, the power has slowly been increased to 303,2 W for 10 min before it was decreased and the power supply was shut off to retrieve the nanofibers. The whole process is schematically shown in Figure 1.

Characterization

A micropyrometer from Pyro-Werke Hannover was used to estimate the temperature inside the CNF during the process by direct comparison with a tungsten wire. It has to be noted that the micropyrometer only operates to a maximum of 3400 °C and that the estimated temperature coming from the comparison of the color of both the tungsten wire in the pyrometer and the CNF's themselves is not equal.

X-ray diffraction was used for the structural characterization of the GNFs, using a Bruker D2 phaser. The samples were scanned from 10° – 80° 2θ with a stepping of 0.04° using Cu-K_α (λ = 1.5406 Å) radiation. The Bragg law $d_{002} = (\lambda/2 \cdot \sin \theta)$ calculates the inter-layer spacing $d(002)$, where θ the Bragg angle. Additionally, the crystallite sizes were estimated using the Scherrer equation $L_c = (K\lambda/(\beta \cos \theta))$, with

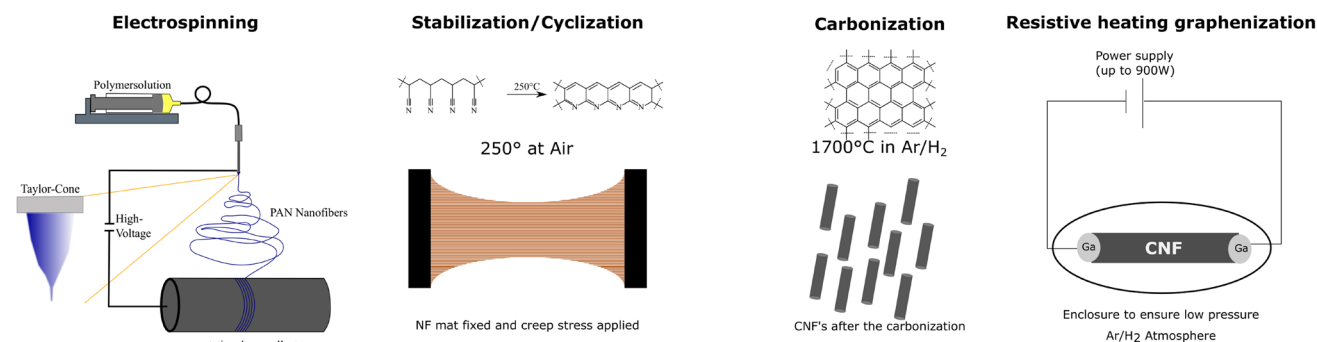


Figure 1 Schematically process of the GNF production.

K as the shape factor (0.89 for L_c) and β being the full width at half maximum (FWHM) of the reflex [23].

For the estimation of the number of graphene layers and to obtain information about the structure, especially disorder or defects in the GNF samples, Raman spectra were recorded using a DXR2 from Thermo Fisher Scientific with a laser wavelength of 532 nm as excitation source. The spectra were recorded in the range of 50–2850 cm^{-1} . The D, G, and 2D-bands of the spectra were deconvoluted using Gaussian fitting via OriginLab pro software. From this, the integral ratios of I_D/I_G and I_{2D}/I_G of the respective bands were calculated as well as the FWHM of the 2D-band. The crystal size L_a of carbon nanostructures has been calculated via $L_a = (2.4 \cdot 10^{-10}) \lambda^4 I_G / I_D$, with λ as the laser wavelength [18, 24, 25].

The degree of hybridization was calculated from sp^2 and sp^3 fraction of the C1s photoemission spectrum taken with XPS using the Al- K_{α} emission and a PHI 5000 VersaProbe III analyzer operating with a pass energy of 27 eV. After subtraction of the Shirley background, the C1s spectra were fitted using symmetric Gaussian–Lorentzian sum functions under the constraint that the energy difference between sp^2 and sp^3 peak is 0.8 eV [26].

The morphology of the nanofibers was analyzed by scanning electron microscopy (SEM) using a Carl Zeiss Supra 55VP. For the measurement of the nanofiber diameter, ImageJ was used and forty readings were taken from seven different SEM images.

The electrical conductivity of the nanofiber mats was measured by a 4-point probe method under ultra-high vacuum using a 4-tip STM/SEM system [27]. The conductivity was calculated from the resistance R including the dimensions of the samples via $\sigma = L / (A_{\text{true}} \cdot R)$, where L is the distance between the probes. The effective area A_{true} was calculated by the division of the linear density of fiber mats by the density of CNF, assumed to be 1.7 g/cm^3 , similar to the density of commercial carbon fibers.

Figure 2 Picture of the GNFs during the self-resistive heating process.



Results and discussion

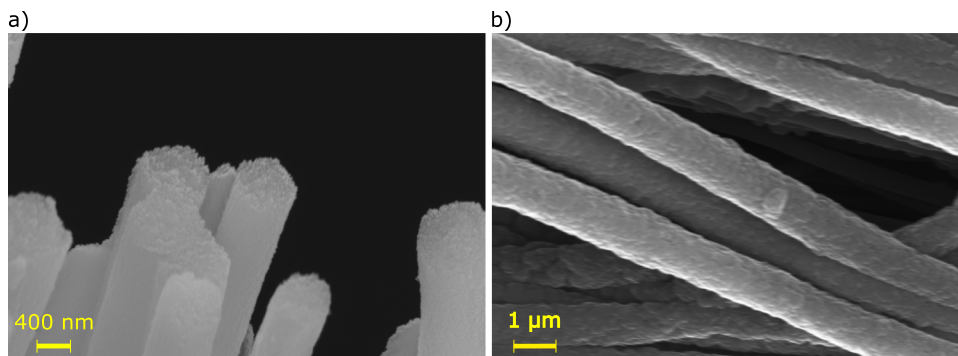
Resistive heating process

During the resistive heating of the GNFs, the micro-pyrometer was positioned to monitor the color change of the nanofibers. For this, the color of the GNFs was matched with the color of the tungsten wire by increasing the potential and current passing through the wire. The resulting power was then converted to the temperature of the wire, which is used to approximate the temperature of the GNFs. As the sublimation temperature of carbon is at $3642 \text{ }^\circ\text{C}$, the temperature was estimated between $3350 \text{ }^\circ\text{C}$ and $3450 \text{ }^\circ\text{C}$. In Figure 2, the GNFs are shown while they are heated. Due to the camera settings, the picture is less bright than it appeared during the experiment. The process in this study was a batch process, but due to the usage of a liquid contact agent such as gallium, this process can quickly be adapted to a semi-continuous process. The CNF will be pulled through the resistive heating zone and achieve the graphenization during the time in the electric circuit. Additionally, this process is more energy efficient as the heat is directly produced from within the fibers and does not need to be transported into the fibers, where a lot of the heat gets lost. More challenging will be implementing the low-pressure reduced atmosphere for a continuous application. As for concerns regarding the safety of operation, they are low, as the temperature comes from the fibers, an advantage regarding environmental concerns, as less energy is required, and can quickly be dissipated by the setup. In case a leak occurs, the fibers will quickly burn because of the oxygen, and the electrical circuit will be open, and the graphenization stops.

Morphology and structure of graphene nanofibers

Figure 3 summarizes SEM images of the GNFs. The two images show the edge of the fiber and an image

Figure 3 SEM images of the GNFs at an acceleration voltage of 20 kV with a view on the cutting edge **a** and along the fibers **b**.



along the fiber axis. The images show a continuous neat fiber structure, with no beading and no sintered fibers. Furthermore, the average diameter of the GNFs was in the range of 600 nm, which is high, coming from the increased polymer concentration in the solution during the first steps of the electrospinning process. The GNFs show no pore system on the surface although the surface is rough. The CNFs prepared at 1700 °C only show a minimally increased average fiber diameter around 640 nm. This comes from the graphenization process in which the shrinkage takes place. Regarding the cutting edge, the CNFs seem to be smoother (see Supporting Information Figure S8), compared to the GNF edge in Figure 3a). This hints at differences in the crystal structure of the fibers.

X-ray diffraction

The effect of the self-resistive heating on the crystallinity was studied using XRD. The diffractograms for CNFs carbonized at 800 °C and 1700 °C and the GNFs are shown in Figure 4. The values for the reflex angle, FWHM, and the calculated inter-layer space and crystallite size L_c can be found in Table 1. It is obvious that the reflex becomes sharper as the FWHM decreases, indicating the high crystallinity of the GNFs. The reflex angle also shifts to higher values and for the GNF with 26.15° comes close to the ideal angle [28]. During carbonization, small crystallites are formed, and stacking of the crystallite planes takes place. Above 1500 °C, the crystallite growth in size takes place, and a long-range ordering occurs. The primary structure of the fibers is composed of bent layers of sp^2 -hybridized carbon atoms, which are disordered in stacking. The calculated inter-layer spacing reinforces this observation as it decreases to a distance of 340 pm. The high crystallite size, calculated by the Scherrer equation, indicates that the GNFs are the

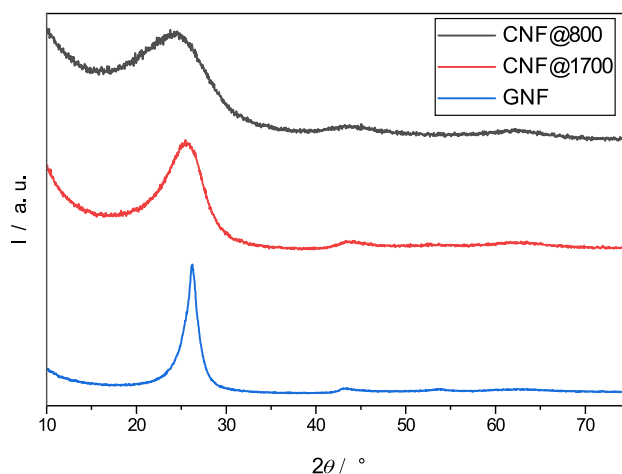


Figure 4 X-ray diffraction pattern of CNF's at different temperatures compared with GNFs.

Table 1 The values of the reflex angle 2θ , FWHM of it, L_c and d_{Bragg} for the samples as calculated from the XRD results

Sample	$2\theta/^\circ$	FWHM/ $^\circ$	L_c/nm	d_{002}/pm
CNF@800	23.69	12.17	0.659	375
CNF@1700	25.24	5.698	1.413	352
GNF	26.15	1.534	5.258	340

most crystalline samples of all the fibers measured. It is visible that the higher carbonization temperature is beneficial to achieve highly crystalline nanofibers and that the trend observed in lower carbonization temperatures (800 °C to 1700 °C) is still valid for higher temperatures.

Raman analysis

Typical Raman spectra for CNFs carbonized at 800 °C and 1700 °C and the GNFs are shown in Figure 5. The

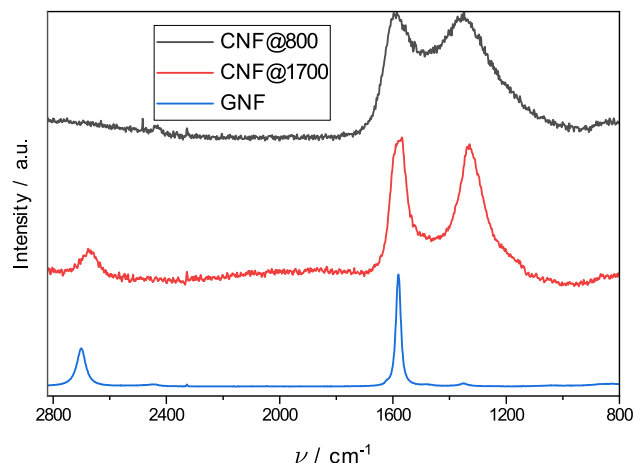


Figure 5 Raman spectra of CNF's at different temperatures compared with GNFs.

two major peaks centering nearly 1360 cm^{-1} and 1585 cm^{-1} in the spectrum are referred to as D- and G-bands, respectively. The G-band is attributed to the in-plane stretching mode of sp^2 -carbon bonds, while the D-band highlights the defects in the graphitic structure [29]. The integral intensity ratio of the D- and G-bands demonstrates the graphitic quality of the samples, while the FWHM of the G-band reflects the degree of graphitization [20]. Additionally, a third peak around 2700 cm^{-1} is referred to as the 2D-band, as it is an overtone of the D-band and results from a two-phonon lattice vibrational process. Its symmetry and FWHM are used to determine the layer thickness of graphene in a sample [19]. For a lower temperature (CNF@800), no 2D-band was observed compared to the samples carbonized at higher temperatures. The D- and G-bands are also overlapping and become isolated from each other with increasing temperature, as well as a decrease in $\frac{I_D}{I_G}$ and decreasing FWHM of all bands. The calculated L_a (domain crystal size along the basal plane) shown in Figure 5b) is also drastically increased for the GNFs, as it is at 546 nm and is fifty times higher than the CNF@1700. Additionally, the ratio of the intensity integrals $\frac{I_D}{I_G}$ for the GNFs is between the calculated values of single-layer and double-layer graphene, indicating a structure of a folded single-layer graphene layout [30]. With a high symmetry of the 2D-band and its low FWHM, displayed in Table 2, it can be concluded that the GNFs are made of single- and few-layer folded graphene domains, as single-layer graphene shows a perfectly symmetrical

2D-band and a FWHM of around 30 cm^{-1} as shown in Figure 6a) [19]. Furthermore, the lack of a D-band and with the peak maxima of the G- and 2D-band at 1581 cm^{-1} and 2701 cm^{-1} , respectively, indicate that the carbon in the fiber structure is highly crystalline and defect-free.

As previously mentioned, temperatures above $1500\text{ }^\circ\text{C}$ lead to size growth and defect healing. During the self-resistive heating, domains with more defects create a higher electrical resistance compared to other fibers, leading to higher temperatures. At the grain boundaries, those temperatures can reach the sublimation temperature of carbon, resulting in the decomposition of high-defect layers and grains. As for the observed GNFs with almost no defects, the structure can continuously grow during the process.

XPS analysis

Furthermore, XPS was performed on all carbon nanofibers to quantify the $\frac{\text{sp}^2}{\text{sp}^3}$ hybridized carbon ratio.

In Figure 6, typical C1s XPS spectra for all samples are shown. The C1s spectra are deconvoluted into two major peaks, namely the sp^2 hybridized carbon atoms at 284.8 eV and sp^3 hybridized carbon atoms at 285.6 eV , and two less intense emissions, namely the shake-up emission at 291.1 eV and C–O emission at 286.8 eV . The latter are not present anymore in the GNF spectra as the graphenization took place above $3000\text{ }^\circ\text{C}$, and the GNF consists of 99.9% carbon. The sp^2 fraction and $\frac{\text{sp}^2}{\text{sp}^3}$ values evaluated are shown in Table 3. Both values increase with higher temperature, as the CNFs exhibit a similar pattern to the results by Ali et al. [2]. The GNFs' sp^2 fraction observed with 88% being the highest value supports the findings from Raman and XRD, where the results showed the formation of high crystalline single- to few-layer graphene nanofibers. It is

Table 2 The values of the FWHM of the 2D peak, ratio of I_D/I_G and I_{2D}/I_G and L_a for the samples as calculated from the Raman results. As there is no 2D peak for the CNF@800, neither FWHM nor I_{2D}/I_G can be calculated and therefore left out empty

Sample	FWHM _{2D} /cm ⁻¹	I_D/I_G	I_{2D}/I_G	L_a/nm
CNF@800		2.93		7
CNF@1700	82.8	1.61	0.24	12
GNF	35.4	0.03	0.61	546

Figure 6 a 2D-band with Fit of the GNFs. Background subtracted XPS spectra of deconvoluted C1s peak for CNF@800 b, CNF@1700 c and GNF d, with fitted peaks of the different bonds of carbon.

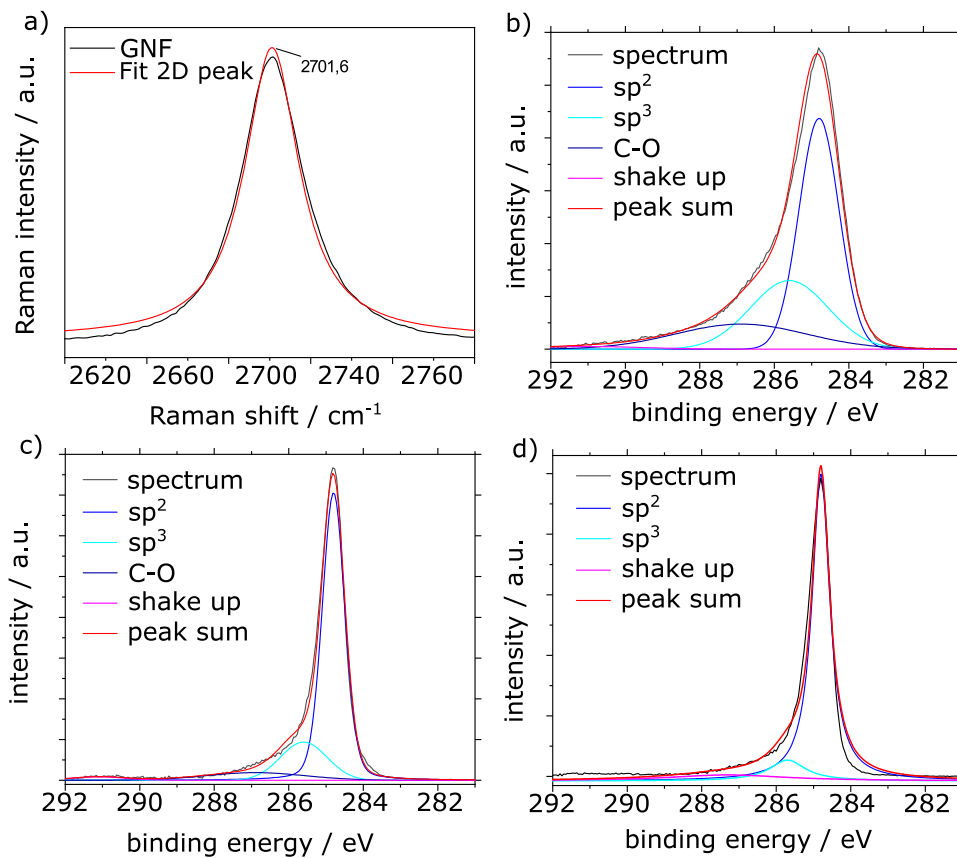


Table 3 Observed sp^2 fraction and $\frac{sp^2}{sp^3}$ ratio for the samples as evaluation of the integrated intensity from the deconvoluted C1s spectra of XPS

Sample	$\frac{sp^2}{sp^3}$ ratio	sp^2 fraction
CNF@800	1.73	50.85 %
CNF@1700	3.99	72.27 %
GNF	7.21	87.82 %

important to note that contrary to the information depth of the Raman, where mainly the findings are of the core of the nanofibers, XPS is a surface-sensitive analysis, with a mean free path length of nearly 10 monolayers. As the findings of both analyses are complementary, it shows a graphitic homogeneity of the GNF throughout the whole nanostructure.

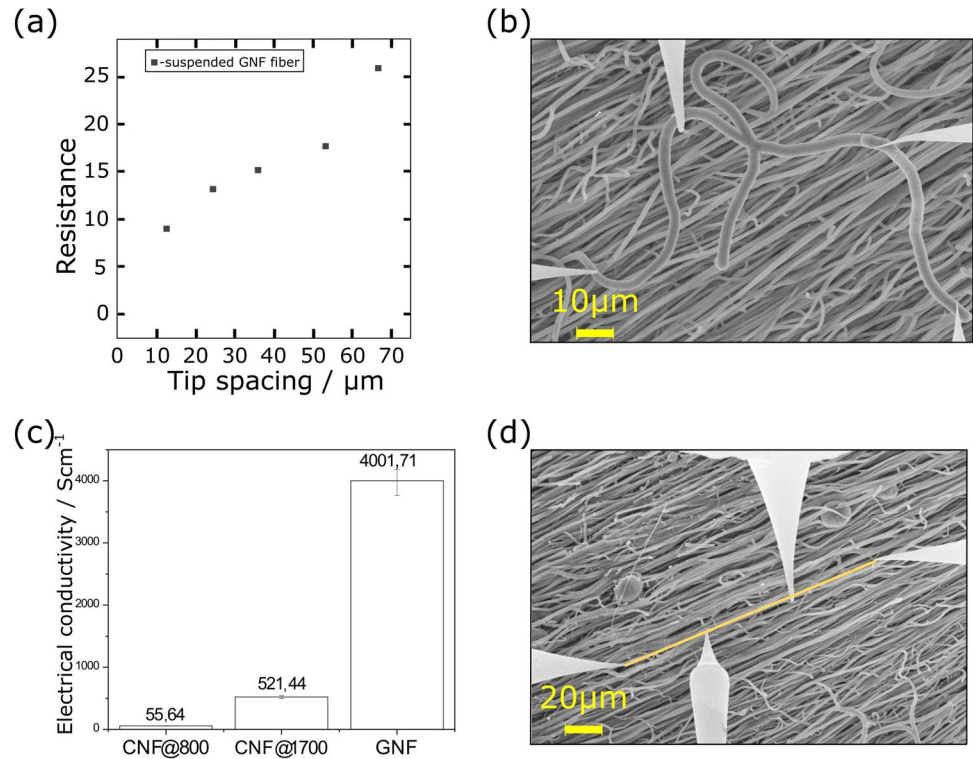
The accumulated evidence strongly supports the utilization of self-resistive heating in CNF transformation through direct electric energy, facilitating the production of GNFs. The integrity of the CNF plays a pivotal in ensuring the quality of the GNF. Even minor

imperfections in the carbon nanofiber structure may induce localized carbon sublimation, thereby destabilizing the overall structure and impeding the flow of current, consequently leading to fiber damage.

Electrical conductivity of GNFs and CNF's

The results of electrical conductivity measurements of the CNFs at different temperatures are shown in Figure 7. The conductivity was measured for all CNFs in the fiber axis direction and is similar to the results previously published by Ali et al. [3]. The GNFs follow the trend of increasing electrical conductivity with increased carbonization temperature. The electrical conductivity of GNFs is $4000 \text{ Sc}^{-1}\text{m}$, eight times greater than that of CNF@1700, while the carbonization temperature is increased only by a factor of 2, suggesting that the structure becomes even more graphitic as supported by XRD and Raman results. Also, the decrease of defects, as visible from the very low D-band for the GNFs, is beneficial to the structure and, therefore, the conductivity. Previous studies explained the electrical transport properties of our 1D

Figure 7 Resistance in dependency of the tip spacing (a). 4-point STM measurement of a suspended fiber at 15 kV (b). Measured bulk electrical conductivity of CNF's at varying carbonization temperatures (c). SEM image during 4-point STM measurement of an embedded fiber along its axis at 15 kV (d).



carbon structures as a cumulative effect of the connection of different crystalline units (sp^2 clusters) and subcrystalline units in an sp^3 -type insulating matrix [2]. The conductivity is explained as a combination of band conductivity in the sp^2 clusters and electron hopping between those clusters [31, 32]. In our case, we drastically increased the size of the sp^2 clusters, as visible via Raman and XPS (Table 2, 3). Reducing the amount of electron hopping leads to the increased conductivity measured for the GNFs. The enhancement of the GNFs' conductivity also stems from the higher degree of sp^2 -hybridized carbon atoms, leading to higher electron delocalization in the graphene plane and resulting in better electron mobility and higher surface electron concentration [33, 34]. The higher conductivity, which leads to fewer thermal problems, as well as the high crystallinity, may be used in batteries or as electrode materials in fuel cells, as similar studies show [35, 36].

In summary, the results of the Raman spectra indicate a few-layer graphene structure, resulting from the small FWHM of the 2D-band and the integral intensities. The conductivity has been increased, showing a significantly higher value than GO or reduced GO [37]; however, compared to CNTs, it is lower [38], but the possibility to have continuous production of the

GNFs shows great potential for future applications. Additionally, this approach makes GO as a precursor material obsolete, which also lowers the production cost of GNFs as well as reduces environmental concerns by removing the need for GO preparation.

Conclusion

In this study, the production of neat graphene nanofibers (GNFs) with improved crystallinity, defect-free structures, and electrical conductivity has been realized. For the in situ synthesis of GNFs, an additional carbonization step with self-resistive heating was used to reach temperatures close to the sublimation temperature of carbon. The microstructure, graphitization, and electrical conductivity were investigated via SEM, XRD, Raman, XPS, and 4-tip STM for the samples, revealing that self-resistive heating at such high temperatures improves the crystalline structure and graphitization degree, producing neat graphene nanofibers using only PAN as precursor material. This facilitates the production of said fibers to an in situ process without using a template like the addition of GO [5], with the following reduction steps. Additionally, compared to reduced GO, in the GNF, it was possible to obtain an

almost defect-free structure, measurable by the low integral intensity of the D-band in the Raman spectra. The analysis of the 2D-band of the Raman spectra indicates a few-layer structure. The FWHM of 35 cm^{-1} is higher than the value for single-layer graphene but much lower than for a double-layer [19]. Therefore, we conclude it to be a single-layer graphene structure that is folded, creating the peak broadening. We suggest them to be similar to nanoscrolls [39], supported by the measured Raman spectra, with little to no defects. The low diameter of the GNFs can be used to work effectively against the skin effect in high-frequency electrical currents. This simple way of producing neat GNFs with a plain polymer solution could lead to easier access to graphene-based nanomaterials and their applications. Especially the conversion of the batch process to a continuous setup by pulling the nanofiber through the heating segment is part of future studies to broaden availability.

Acknowledgements

The authors would thank the Hannover school for nanotechnology (hsn), the Leibniz Universität Hannover (LUH), the Laboratory of Nano and Quantum Engineering (LNQE), for the XPS measurements.

Authors contributions

Conceptualization, methodology, validation, formal analysis, and writing—original draft preparation were performed by Jules Brehme; investigation was done by Jules Brehme and Markus Gruschwitz; writing—review and editing was performed by Christoph Tegenkamp, Franz Renz, and Ralf Franz Sindelar. All authors have read and agreed to the published version of the manuscript.

Funding

Open Access funding enabled and organized by Projekt DEAL.

Data availability

Data will be provided upon reasonable request.

Declarations

Conflict of interests The authors declare that they have no known competing financial interests or personal relationships that could have appeared to influence the work reported in this paper.

Supplementary Information The online version contains supplementary material available at <https://doi.org/10.1007/s10853-025-11084-1>.

Open Access This article is licensed under a Creative Commons Attribution 4.0 International License, which permits use, sharing, adaptation, distribution and reproduction in any medium or format, as long as you give appropriate credit to the original author(s) and the source, provide a link to the Creative Commons licence, and indicate if changes were made. The images or other third party material in this article are included in the article's Creative Commons licence, unless indicated otherwise in a credit line to the material. If material is not included in the article's Creative Commons licence and your intended use is not permitted by statutory regulation or exceeds the permitted use, you will need to obtain permission directly from the copyright holder. To view a copy of this licence, visit <http://creativecommons.org/licenses/by/4.0/>.

References

- [1] Paillet M, Parret R, Sauvajol J-L, Colombari P (2018) Graphene and related 2d materials: An overview of the raman studies. *J Raman Spectrosc* 49(1):8–12. <https://doi.org/10.1002/jrs.5295>
- [2] Ali AB, Slawig D, Schlosser A, Koch J, Bigall NC, Renz F, Tegenkamp C, Sindelar RF (2021) Polyacrylonitrile (PAN) based electrospun carbon nanofibers (ECNFs): Probing the synergistic effects of creep assisted stabilization and CNTs addition on graphitization and low dimensional electrical transport. *Carbon* 172:283–295. <https://doi.org/10.1016/j.carbon.2020.10.033>
- [3] Ali AB, Renz F, Koch J, Tegenkamp C, Sindelar R (2020) Graphene Nanoplatelet Doped Carbon Nanofiber System: Effect of GNPs on the Graphitic Structure of Creep Stress and Non-Creep Stress Stabilized Polyacrylonitrile. *Nanomaterials* 10(2):351–366. <https://doi.org/10.3390/nano10020351>

- [4] Xin G, Yao T, Sun H, Scott SM, Shao D, Wang G, Lian J (2015) Highly thermally conductive and mechanically strong graphene fibers. *Mater Sci* 349(6252):1083–1087. <https://doi.org/10.1126/science.aaa6502>
- [5] Han Z, Wang J, Liu S, Zhang Q, Liu Y, Tan Y, Luo S, Guo F, Ma J, Li P, Ming X, Gao C, Xu Z (2022) Electrospinning of Neat Graphene Nanofibers. *Adva Fiber Mater* 4:268–279. <https://doi.org/10.1007/s42765-021-00105-8>
- [6] Kilpakja S, Schmid SR (2019) *Manufacturing Engineering and Technology*. Pearson
- [7] Ali AB, Renz F, Dreyer B, Tegenkamp C, Sindelar R (2018) Electrospun Polyacrylonitrile Based Carbon Nanofibers: The Role of Creep Stress towards Cyclization and Graphitization. *J Mater Sci Eng* 7(493):1–8. <https://doi.org/10.4172/2169-0022.1000493>
- [8] Kilic MS, Brehme J, Pawlak J, Tran K, Bauer F, Shiga T, Suzuki T, Nihei M, Sindelar RF, Renz F (2023) Incorporation and Deposition of Spin Crossover Materials into and onto Electrospun Nanofibers. *Polymers* 15(10):2365. <https://doi.org/10.3390/polym15102365>
- [9] Wang Y, Xu Y, Zhai W, Zhang Z, Liu Y, Cheng S, Zhang H (2022) In-situ growth of robust superlubricated nanoskin on electrospun nanofibers for post-operative adhesion prevention. *Nat Commun* 13(1):5056
- [10] Li J, Lin H, Li J, Wang Y (2024) Engineered lubricative lecithin-based electrospun nanofibers for the prevention of postoperative abdominal adhesion. *Pharmaceutics* 16(12):1562
- [11] Yin Y, Guo C, Mu Q, Li W, Yang H, He Y (2024) Dual-sensing nano-yarns for real-time pH and temperature monitoring in smart textiles. *Chem Eng J* 500:157115
- [12] Günther A, Deja Y, Kilic M, Tran K, Kotra P, Renz F, Kowalsky W, Roth B (2024) Investigation of the molecular switching process between spin crossover states of triazole complexes as basis for optical sensing applications. *Sci Rep* 14(1):5897
- [13] Kilic MS, Brehme J, Deja Y, Pawlak J, Günther A, Sander A, Müller D, Renz A, Rajnak C, Polášková M et al (2024) Thin films with implemented molecular switches for the application in polymer-based optical waveguides. *Interactions* 245(1):8
- [14] Novoselov KS, Geim AK, Morozov SV, Jiang D, Zhang Y, Dubonos SV, Grigorieva IV, Frisov AA (2004) Electric Field effect in Atomically Thin carbon films. *Science* 306(5696):666–669. <https://doi.org/10.1126/science.1102896>
- [15] Geim AK, Novoselov KS (2007) The rise of graphene. *Nat Mater* 6(3):183–191
- [16] Novoselov KS, Falco VI, Colombo L, Gellert PR, Schwab MG, Kim K (2012) A roadmap for graphene. *Nature* 490(7419):192–200
- [17] Zhang Y-H, Chen Y-B, Zhou K-G, Liu C-H, Zeng J, Zhang H-L, Peng Y (2009) Improving gas sensing properties of graphene by introducing dopants and defects: a first-principles study. *Nanotechnology* 20:185504. <https://doi.org/10.1088/0957-4484/20/18/185504>
- [18] Isaac Childres, Childres Isaac, Jauregui Luis A, Park Wonjun, Cao Helin, Chen Yong P et al (2013) Raman spectroscopy of graphene and related materials. *New Dev Photon Mater Res* 1:1–20
- [19] Hao Y, Wang Y, Wang L, Ni Z, Wang Z, Wang R, Koo CK, Shen Z, Thong JTL (2010) Probing Layer Number and Stacking Order of Few-Layer Graphene by Raman Spectroscopy. *Small* 6(2):195–200. <https://doi.org/10.1002/sml.200901173>
- [20] Ferrari AC, Meyer JC, Scardaci V, Casiraghi C, Lazzeri M, Mauri F, Piscanec S, Jiang D, Novoselov KS, Roth S, Geim AK (2006) Raman Spectrum of Graphene and Graphene Layers. *Phys Rev Lett*. <https://doi.org/10.1103/PhysRevLett.97.187401>
- [21] Liang T, Kong Y, Chen H, Xu M (2016) From solid carbon sources to graphene. *Chin J Chem* 34(1):32–40. <https://doi.org/10.1002/cjoc.201500429>
- [22] Byun S-J, Lim H, Shin G-Y, Han T-H, Oh SH, Ahn J-H, Choi HC, Lee T-W (2011) Graphenes converted from polymers. *J Phys Chem Lett* 2(5):493–497. <https://doi.org/10.1021/jz200001g>
- [23] Zickler GA, Smarsly B, Gierlinger N, Peterlik H, Paris O (2006) A reconsideration of the relationship between the crystallite size L_a of carbons determined by X-ray diffraction and Raman spectroscopy. *Carbon* 44:3239–3242. <https://doi.org/10.1016/j.carbon.2006.06.029>
- [24] Wu J-B, Lin M-L, Cong X, Liu H-N, Tan P-H (2018) Raman spectroscopy of graphene-based materials and its applications in related devices. *Chem Soc Rev* 47(5):1822–1873. <https://doi.org/10.1039/C6CS00915H>
- [25] Tunistra F, Koenig JL (1970) Raman Spectrum of Graphite. *J Chem Phys* 53(3):1126–1130. <https://doi.org/10.3390/polym15102365>
- [26] Mérel P, Tabbal M, Chaker M, Moisa S, Margot J (1998) Direct evaluation of the sp^3 content in diamond-like-carbon films by xps. *Appl Surf Sci* 136(1):105–110. [https://doi.org/10.1016/S0169-4332\(98\)00319-5](https://doi.org/10.1016/S0169-4332(98)00319-5)
- [27] Miccoli I, Edler F, Pfnür H, Tegenkamp C (2015) The 100th anniversary of the four-point probe technique: the role of probe geometries in isotropic and anisotropic systems. *J Phys: Condens Matter* 27(22):223201

- [28] Jiao X, Qiu Y, Zhang L, Zhang X (2017) Comparison of the characteristic properties of reduced graphene oxides synthesized from natural graphites with different graphitization degrees. *RSC Adv* 7(82):52337–52344
- [29] Reich S, Thomsen C (2004) Raman spectroscopy of graphite. *Philos Trans R Soc London. Ser A: Math, Phys Eng Sci* 362(1824):2271–2288
- [30] Kim K, Coh S, Tan LZ, Regan W, Yuk JM, Chatterjee E, Crommie M, Cohen ML, Louie SG, Zettl A (2012) Raman spectroscopy study of rotated double-layer graphene: misorientation-angle dependence of electronic structure. *Phys Rev Lett* 108(24):246103. <https://doi.org/10.1103/PhysRevLett.108.246103>
- [31] Cai J, Chawla S, Naraghi M (2014) Piezoresistive effect of individual electrospun carbon nanofibers for strain sensing. *Carbon* 77:738–746
- [32] Carey J, Silva S (2004) Disorder, clustering, and localization effects in amorphous carbon. *Phys Rev B* 70(23):235417
- [33] Gong P, Yang Y-Y, Ma W-D, Fang X-Y, Jing X-L, Jia Y-H, Cao M-S (2021) Transport and recombination properties of group-iii doped sicnts. *Phys E: Low-Dimens Syst Nanostruct* 128:114578
- [34] Li Y-J, Li S-L, Gong P, Li Y-L, Fang X-Y, Jia Y-H, Cao M-S (2018) Effect of surface dangling bonds on transport properties of phosphorous doped sic nanowires. *Phys E: Low-Dimens Syst Nanostruct* 104:247–253
- [35] Bao L, Zang J, Li X (2011) Flexible zn₂sno₄/mno₂ core/shell nanocable- carbon microfiber hybrid composites for high-performance supercapacitor electrodes. *Nano Lett* 11(3):1215–1220
- [36] Zhang Y, Gao Z, Song N, He J, Li X (2018) Graphene and its derivatives in lithium-sulfur batteries. *Mater Today Energy* 9:319–335
- [37] Jaafar E, Kashif M, Sahari SK, Ngaini Z (2018) Study on morphological, optical and electrical properties of graphene oxide (go) and reduced graphene oxide (rgo). In: *Materials Science Forum*, vol. 917, pp 112–116. *Trans Tech Publ*
- [38] Hong S, Nam J, Park S, Lee D, Park M, Lee DS, Kim ND, Kim D-Y, Ku B-C, Kim YA et al (2021) Carbon nanotube fibers with high specific electrical conductivity: synergistic effect of heteroatom doping and densification. *Carbon* 184:207–213
- [39] Islam M, Rahman MM, Chowdhury MM, Alam MK (2019) Graphene nanoscrolls via electric-field-induced transformation of water-submerged graphene nanoribbons for energy storage, nanofluidic, and nanoelectronic applications. *ACS Appl Nano Mater* 2(9):5857–5870
- [40] De Volder MF, Tawfick SH, Baughman RH, Hart AJ (2013) Carbon nanotubes: present and future commercial applications. *Science* 339(6119):535–539

Publisher's Note Springer Nature remains neutral with regard to jurisdictional claims in published maps and institutional affiliations.